

Supporting Information

Tuning stiffness of mechanical metamaterial unit cells via transitions to second-order rigid and pre-stressed states

Joseph C. Roback, Arya Nagrath, Sameera Kristipati, Christian D. Santangelo, Ryan C. Hayward**

J. Roback, A. Nagrath, S. Kristipati, R.C. Hayward*

Department of Chemical and Biological Engineering, University of Colorado Boulder, Boulder, Colorado, 80303, United States

Email: ryan.hayward@colorado.edu

R.C. Hayward*

Materials Science and Engineering Program, University of Colorado Boulder, Boulder, Colorado, 80303, United States

Email: ryan.hayward@colorado.edu

C.D. Santangelo*

Department of Physics, Syracuse University, Syracuse, New York, 13244, United States

Email: cdsantan@syr.edu

*Corresponding authors

Second order rigidity and geometric rigidification

Our metamaterial takes advantage of the idea of second-order rigidity to achieve its responsiveness. The basic formulation is laid out in several publications,^{1,2} but we summarize the main results here. Let δX_n be the displacement of the vertex n , and L_α be the length of edge α as a function of the vertex positions. A zero mode is defined by nonzero solutions to the equation

$$\sum_n \delta X_n \cdot \nabla_n L_\alpha = 0 \quad (S1)$$

When there are no solutions, δX_n , to Eq. (S1), the system is rigid. This is the situation when the edge lengths of the material are shorter than their critical value, l_c .

A self-stress, σ_α , is defined as the nonzero solutions to

$$\sum_\alpha \sigma_\alpha \nabla_n L_\alpha = 0 \quad (S2)$$

A self-stress is a set of tensions on the edges such that the forces on the vertices are balanced. When $l = l_c$, there is a nontrivial solution to both Eq. (S1) and a solution to Eq. (S2). When this occurs, a necessary condition for a zero mode to extend to a motion of the system is

$$\sum_{\alpha nm} \sigma_\alpha (\delta X_n \cdot \nabla_n) (\delta X_m \cdot \nabla_m) L_\alpha = 0 \quad (S3)$$

If Eq. (S3) has no solution for a zero mode, δX_n , then the system is “second order rigid” or, more specifically, “prestress stable.”² When this occurs, a deformation of the structure increases the length of the edges to quadratic, rather than linear, order.

When the length of the edges in the material is further decreased, there is both a self-stress and physical prestress, $\bar{\sigma}_\alpha$, on the edges that is proportional to the self-stress. It is shown in ref. 1 that an arbitrary deformation δX_n has the form

$$\Delta E = (1/2) \sum_\alpha \sum_{nm} (\delta X_n \cdot \nabla_n L_\alpha) (\delta X_m \cdot \nabla_m L_\alpha) + \bar{\sigma}_\alpha (\delta X_n \cdot \nabla_n) (\delta X_m \cdot \nabla_m) L_\alpha \quad (S4)$$

If the system is second-order rigid, expression (S4) is positive-definite for all deformations, δX_n . Consequently, the system is elastic. These equations justify the picture of Figure 1A, in which there is a transition from an elastic (*i.e.* rigid) to a floppy state as the edge length increases above the critical length.

Mathematical analysis of zero modes and self-stresses

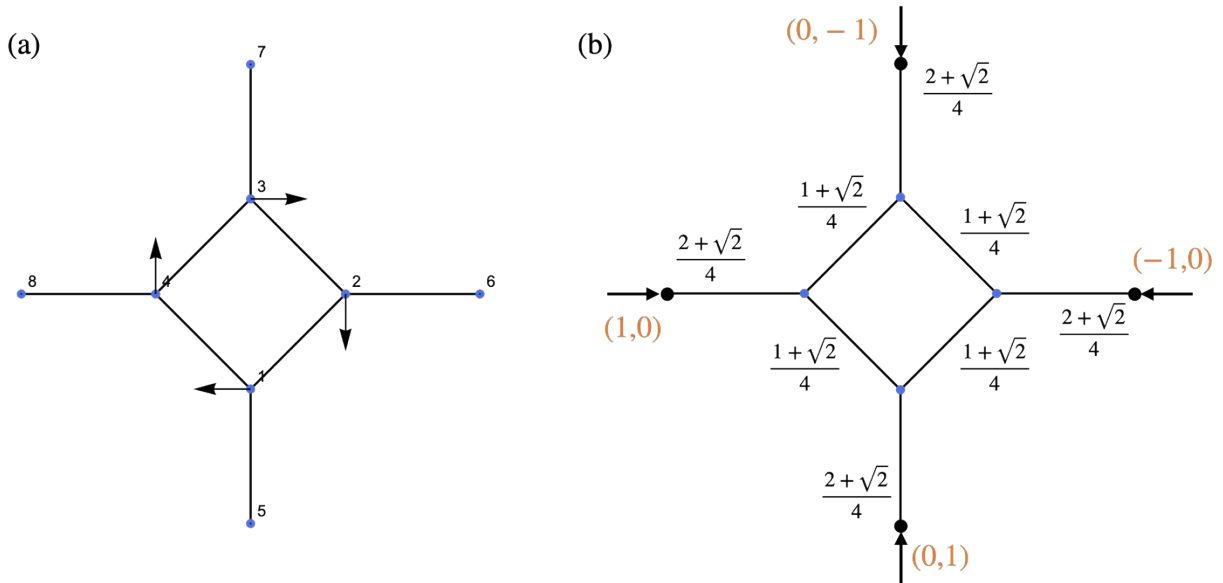


Figure S1. A) When we fix vertices 5 – 8, the unit cell in its critical state has one zero mode. B) Edges are labeled by a self-stress and fixed vertices by the required constraint force.

We analyze the system in two parts. In the first, we consider only the bars inside the fixed frame. The vertex positions and zero mode are:

Vertex	Position	Zero mode
1	$[0, -1/(1 + \sqrt{2})]$	$[-1, 0]$
2	$[1/(1 + \sqrt{2}), 0]$	$[0, -1]$
3	$[0, 1/(1 + \sqrt{2})]$	$[1, 0]$
4	$[-1/(1 + \sqrt{2}), 0]$	$[0, 1]$
5	$[0, -1]$	$[0, 0]$
6	$[1, 0]$	$[0, 0]$
7	$[0, 1]$	$[0, 0]$
8	$[-1, 0]$	$[0, 0]$

Table S1. The vertex positions of the inside of the critical network and the zero mode that occurs when vertices 5-8 are fixed.

The self-stresses are indicated in Fig. S1B. Note that the self-stress components are all positive; in this case, there is no nontrivial solution to Eq. (S3) so the system is prestress stable.²

To analyze the system with the frame, we create additional bars as shown in Fig. S2B and fix vertices 9 and 5 to freeze out Euclidean motions. There are now two zero modes corresponding to the rotation in Fig. S2A and a shearing of the frame.

Vertex	Position	Zero mode 1	Zero mode 2
1	$[0, -1/(1 + \sqrt{2})]$	$[-1, 0]$	$[-1, 0]$
2	$[1/(1 + \sqrt{2}), 0]$	$[0, -1]$	$[-1, 0]$
3	$[0, 1/(1 + \sqrt{2})]$	$[1, 0]$	$[-1, 0]$
4	$[-1/(1 + \sqrt{2}), 0]$	$[0, 1]$	$[-1, 0]$
5	$[0, -1]$	$[0, 0]$	$[0, 0]$
6	$[1, 0]$	$[0, 0]$	$[-1, 0]$
7	$[0, 1]$	$[0, 0]$	$[-2, 0]$
8	$[-1, 0]$	$[0, 0]$	$[-1, 0]$
9	$[-1, -1]$	$[0, 0]$	$[0, 0]$
10	$[1, -1]$	$[0, 0]$	$[0, 0]$
11	$[0, -11/10]$	$[0, 0]$	$[0, 0]$
12	$[-1, 1]$	$[0, 0]$	$[-2, 0]$
13	$[1, 1]$	$[0, 0]$	$[-2, 0]$
14	$[0, 11/10]$	$[0, 0]$	$[-2, 0]$
15	$[-11/10, 0]$	$[0, 0]$	$[-1, -1/10]$
16	$[11/10, 0]$	$[0, 0]$	$[-1, 1/10]$

Table S2. The vertex positions of the critical network and the zero modes of the framed unit cell.

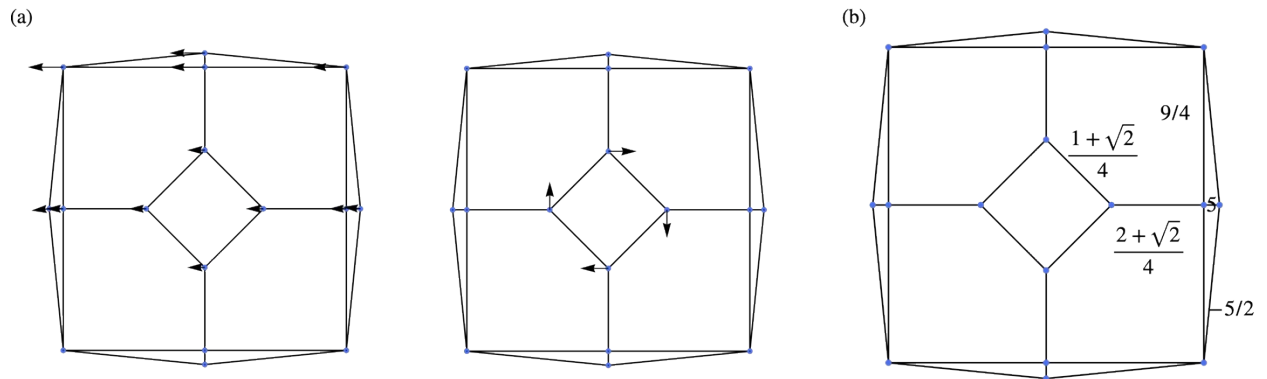


Figure S2. A) Zero modes of framed unit cell. B) Edges are labeled by unique self-stresses of framed unit cells. The self-stresses on the other edges can be found by rotating and reflecting the provided self-stresses.

While in S2B, there are a few negative self-stress components, the self-stress components in the interior are the same as in Fig. S1b and the negative self-stress components only exist in the rigid triangles in the frame. Therefore, Eq. (S3) still has no nonzero solutions, indicated the system is still prestress stable.

The position of the four vertices on the edge of the frame are fixed to match a specific shear angle and the energy is minimized by conjugate gradient. To speed this up and improve errors, we change the shear angle and use the results from the previous minimization as a seed for the next minimization. When $l > l_c$, there is no self-stress in an undeformed frame. However, there is a critical angle, θ , at which the edges begin to stretch again. This is seen in Fig. S3, which plots the energy with respect to the angle, θ . Notice that the critical angle depends on the precise value of l .

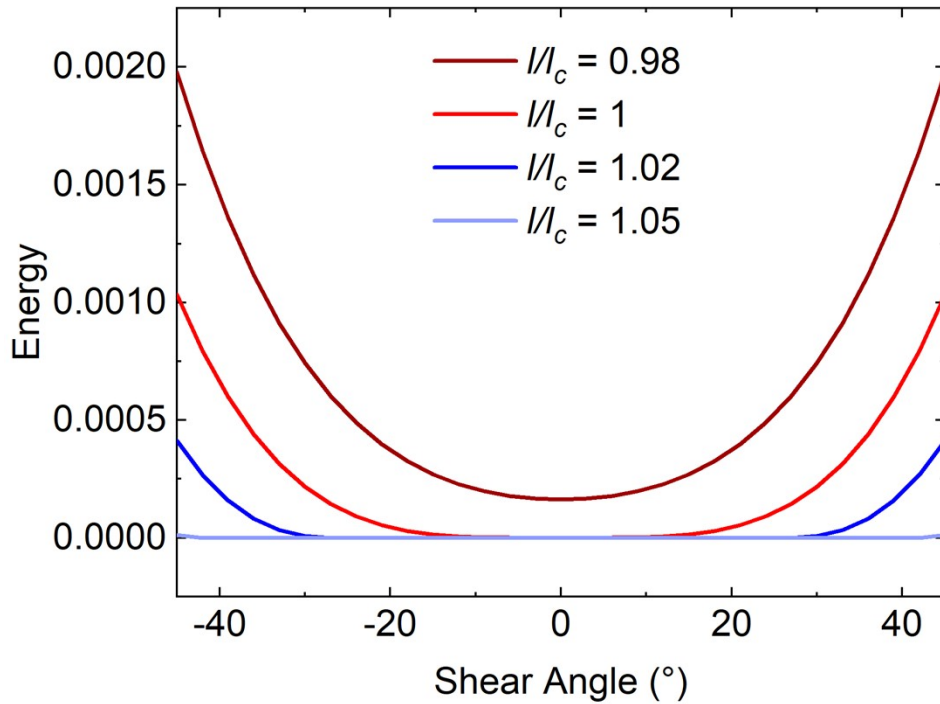


Figure S3. Elastic energy vs. shear angle determined by numerical minimization for unit cells where the joints have zero torsional stiffness (freely rotating). Beyond the critical length, the onset of strain stiffening can be tuned by relatively small increases in beam lengths.

Estimation of bending and stretching stiffness

A replica of a single joint connected by two beams was 3D printed from elastic resin in the same way as the larger unit cell (Figure S4A). Lego hinges are added to each end so that they can freely rotate outside of the clamps. When pulled in tension, the joint first straightens out then begins to stretch, approximating the behavior in the larger unit cells. By measuring the stiffness in each regime, the bending and stretching stiffness of the joints can be estimated.

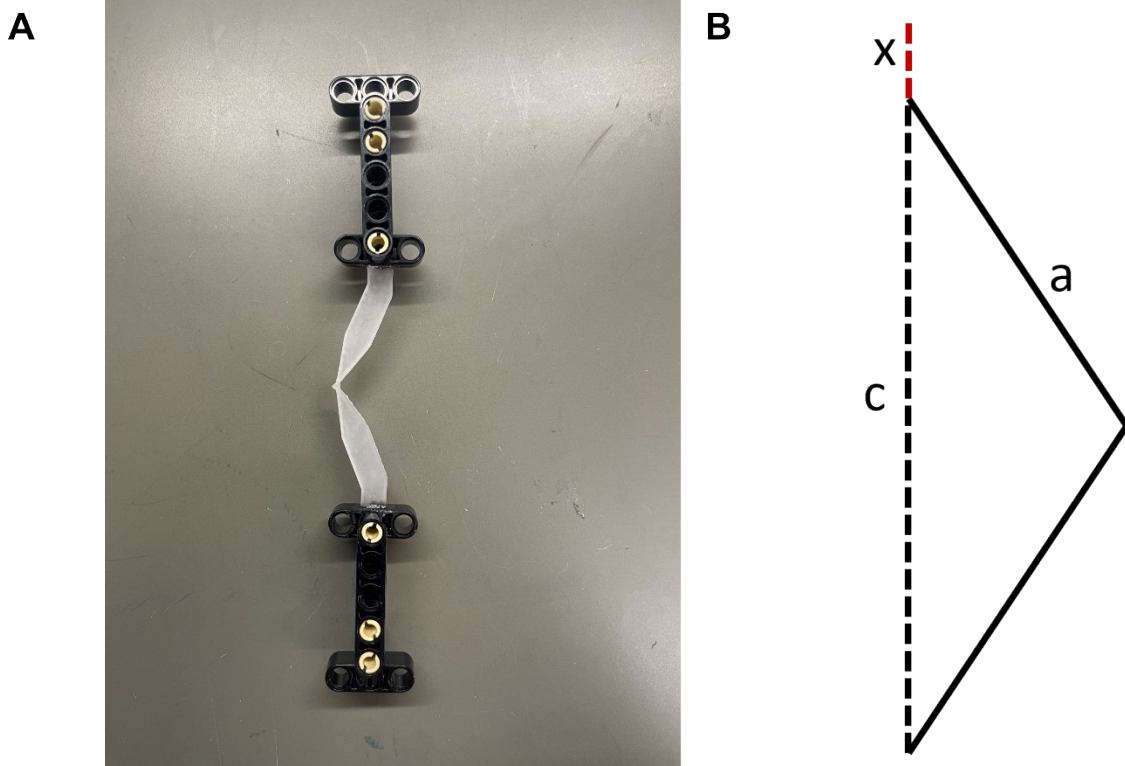


Figure S4. A) Image of 3D printed joint replica. B) Schematic of geometric parameters used to describe the bending stiffness of the joint.

The initial angle of the joint replica is 135° , and the beam length and vertical distance between the two ends are denoted a and c , respectively, as shown in Figure S4B, thus the deviation, γ , from this initial joint angle can be described by the law of cosines:

$$\cos\left(\frac{3\pi}{4} + \gamma\right) = 1 - \frac{(x + c)^2}{2a^2}$$

Expansion of the cosine and quadratic term to first order yields:

$$x \sim \frac{a^2}{\sqrt{2}c} \gamma$$

Thus, the torsional spring constant, k_t , is given by:

$$k_t = \frac{a^2}{\sqrt{2c}}k$$

where k is the slope of the force-displacement curve in the bending regime. Figure S5 shows the measured force-displacement curve for the joint replica. Linear fitting of the stretching regime yields a stretching stiffness of ≈ 590 N/m, and applying the above transformation to the slope of the bending regime yields a bending stiffness of ≈ 0.0437 N/radian. These results were used as model parameters in Figure 1B.

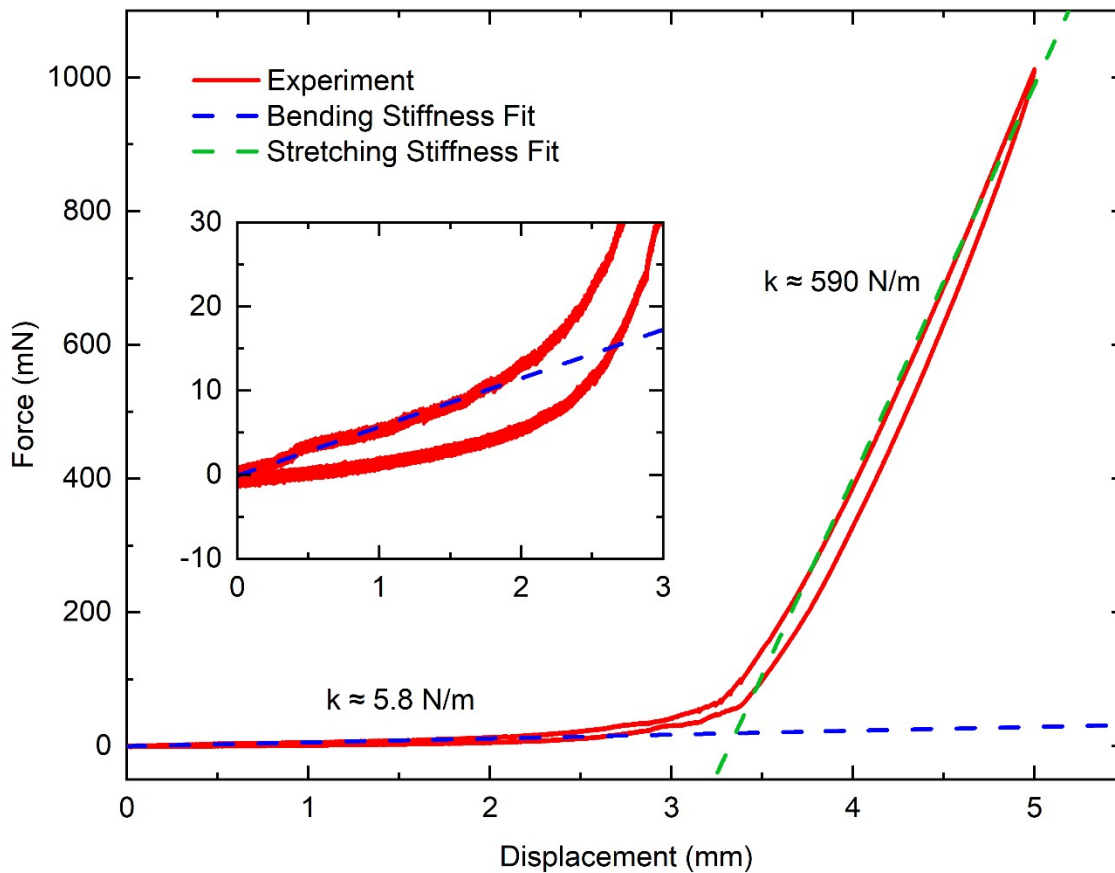


Figure S5. Force-displacement curve for joint replica with linear fits to determine bending vs. stretching stiffness.

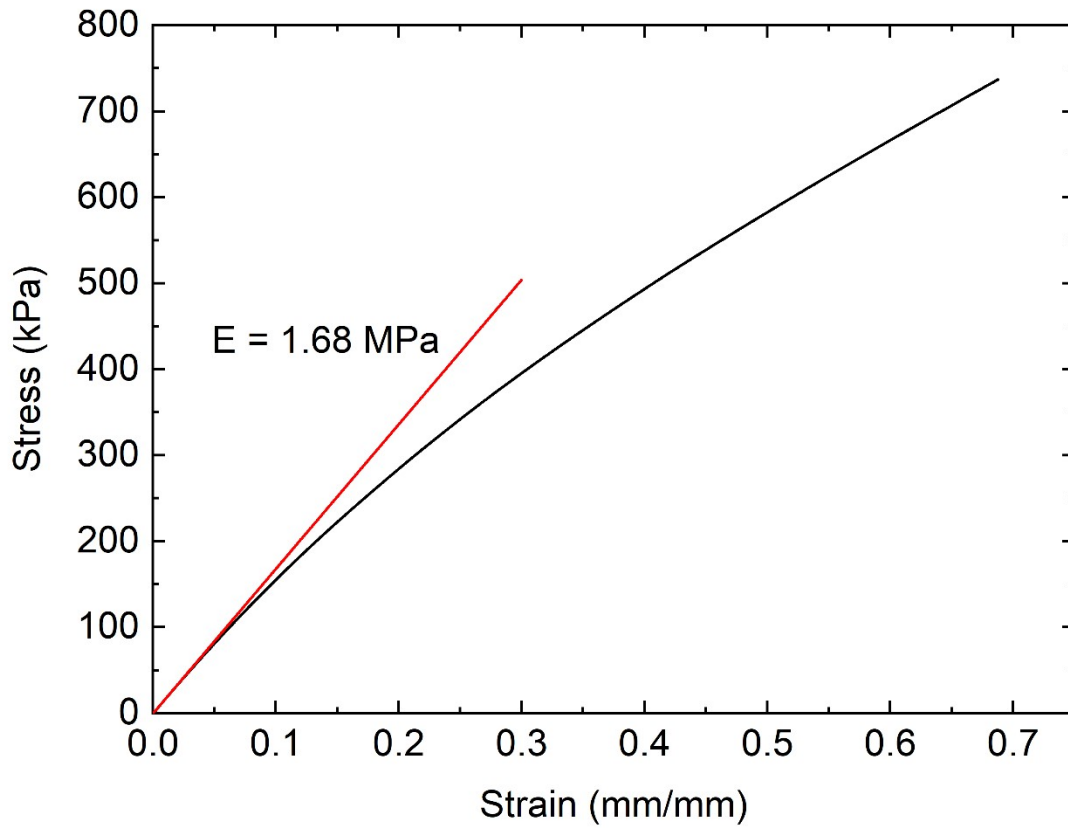


Figure S6. Experimental stress-strain curve for Formlabs Elastic 50A resin including a linear fit for Young's Modulus (red line)

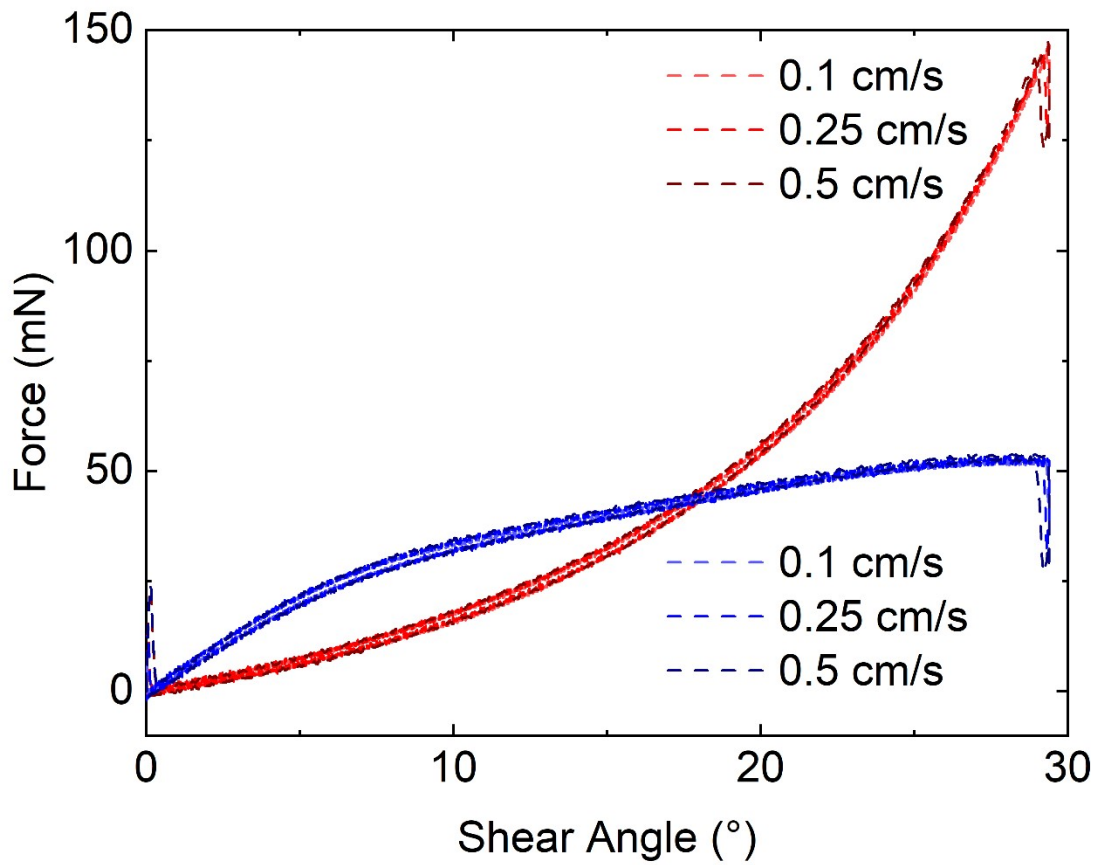


Figure S7. Force displacement curves for 3D printed unit cells at multiple test speeds. The response was found to have a negligible dependence on rate

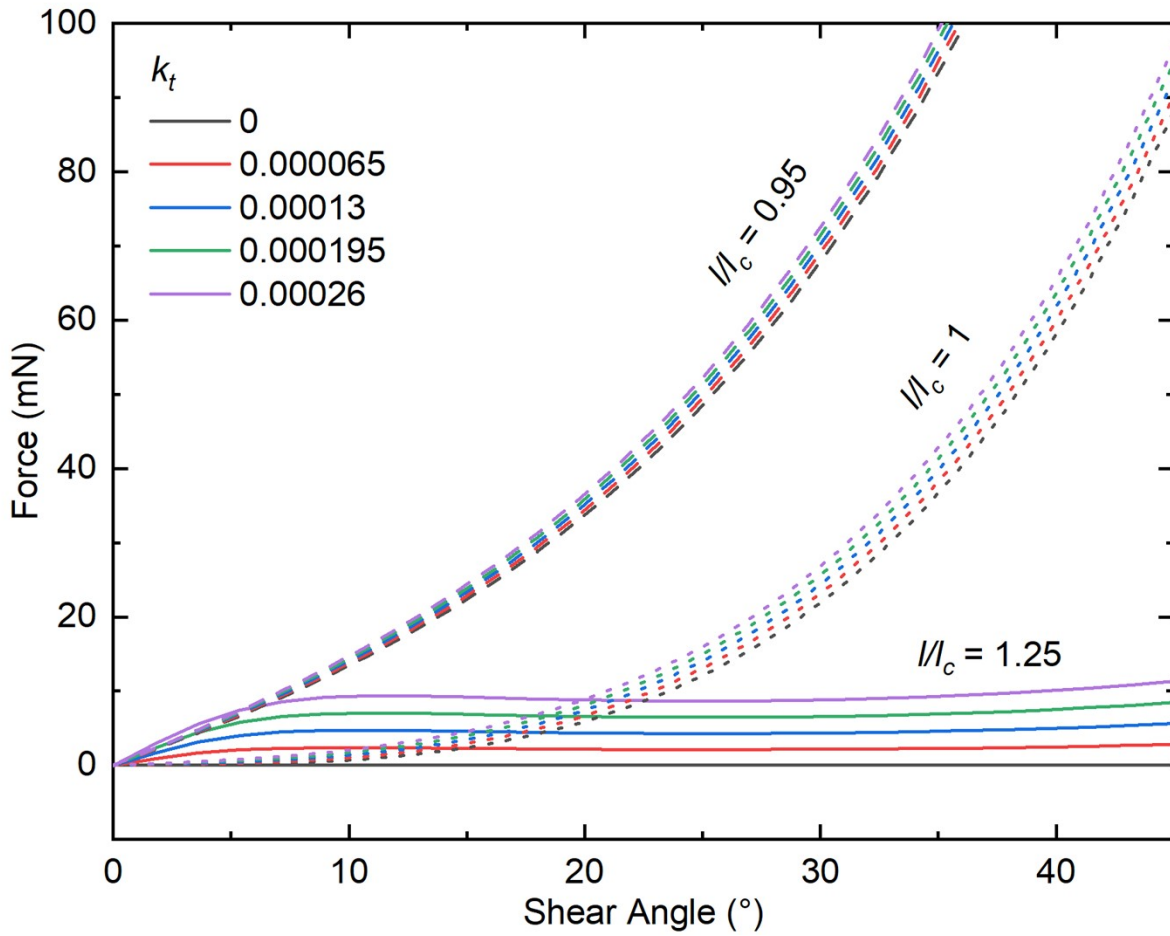


Figure S8. Modelled effect of increasing the torsional stiffness of the metamaterial joints on the force vs. shear response. The floppy configuration ($l/l_c = 1.25$) is given by solid lines, the critical point geometry ($l/l_c = 1$) is given by dotted lines, and the prestressed configuration ($l/l_c = 0.95$) is given by dashed lines.

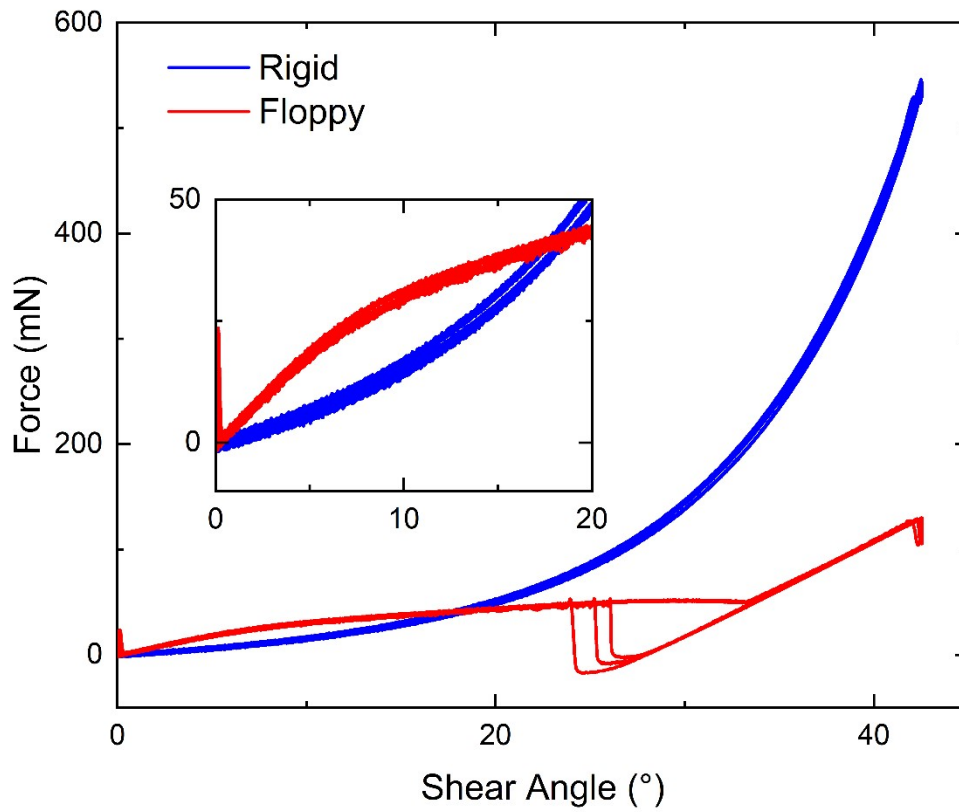


Figure S9. Force vs. shear angle for monolithically 3D printed unit cells, showing that at high shear angles ($\approx 33^\circ$ in this case), self-contact occurs, leading to stiffening of the mechanical response. On unloading, sticking is observed.

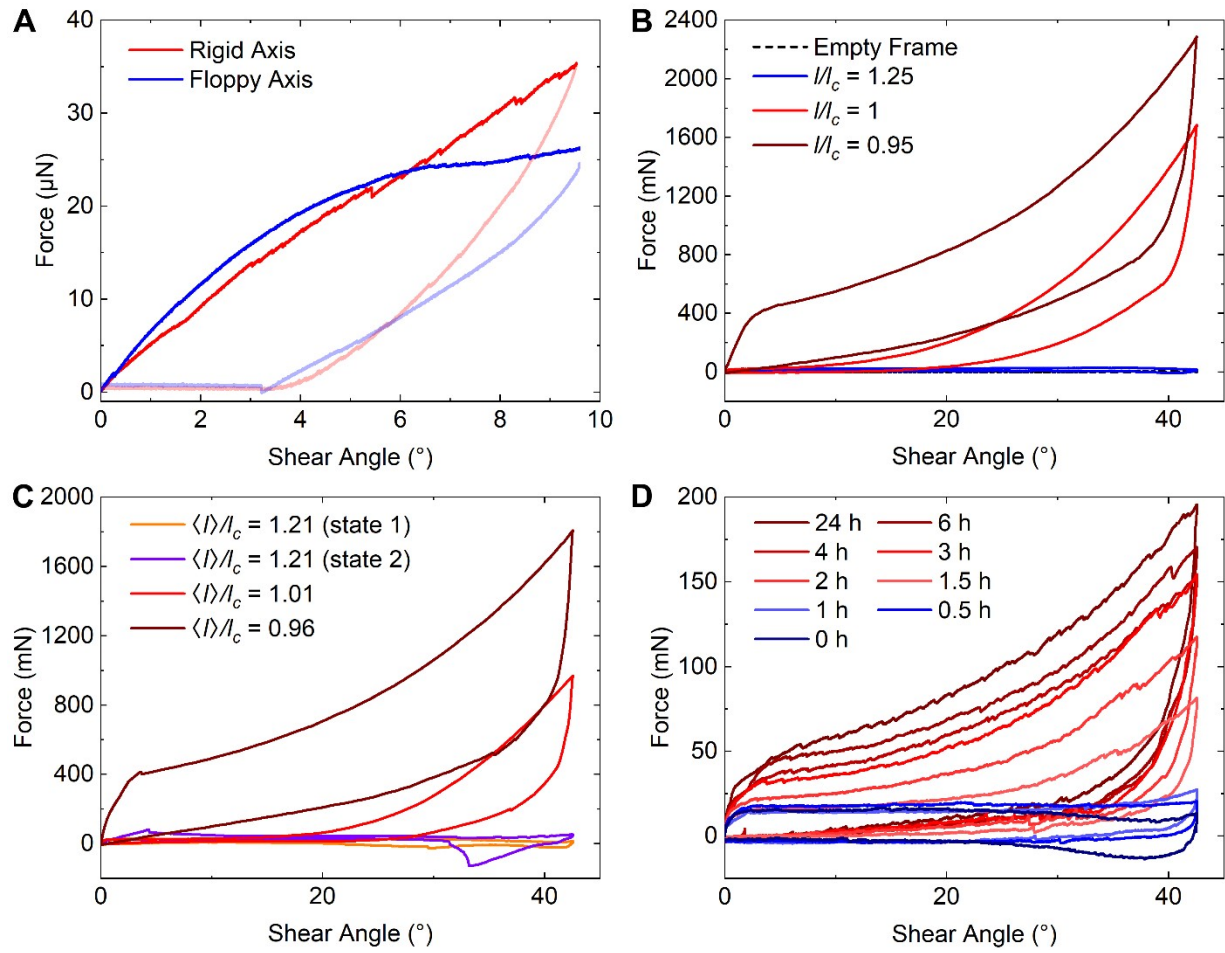


Figure S10. Force vs. shear angle with included unloading curves corresponding to the data in A) Figure 2E, B) Figure 3C, C) Figure 4B, and D) Figure 5D.

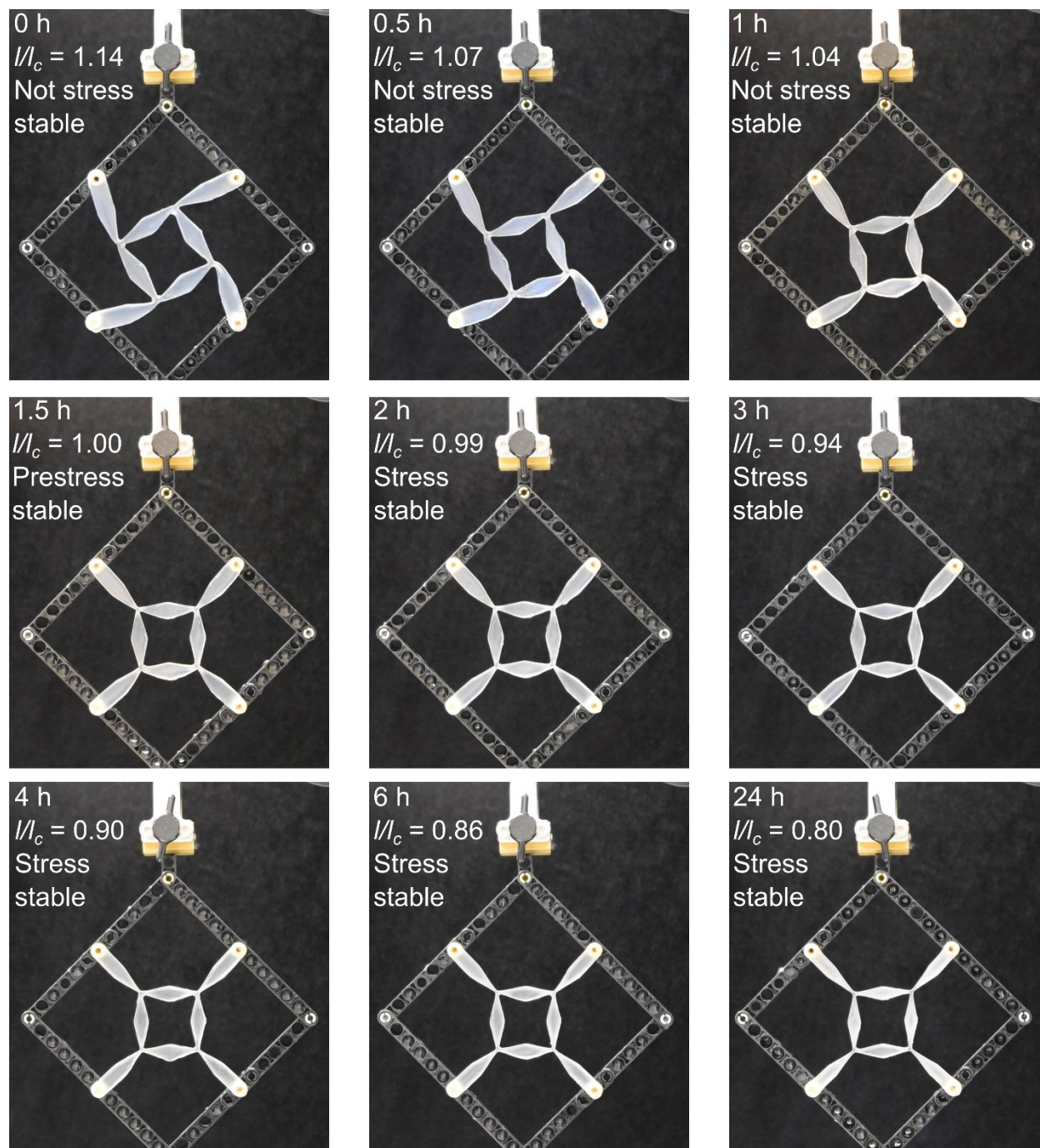


Figure S11. Photographs of Lego/NIPAM hybrid unit cells after immersion in 34°C DI water for each indicated amount of time. Included are also values for l/l_c at that time and the stress stability of the structure.

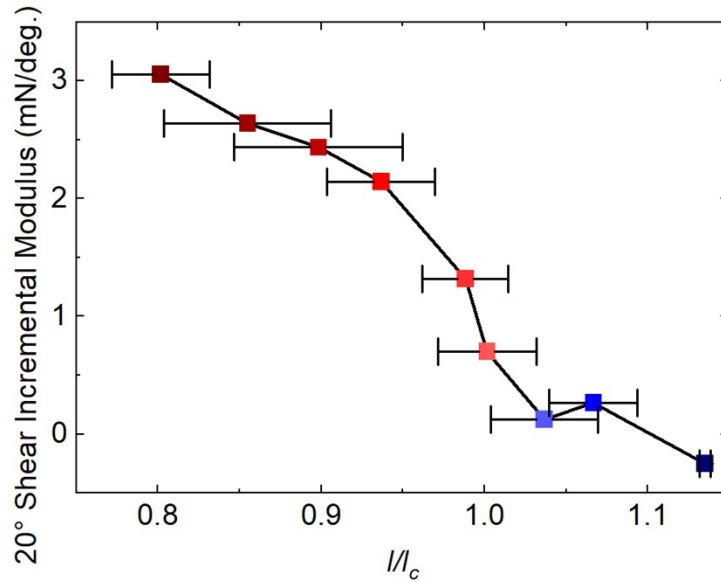


Figure S12. Incremental modulus, defined as the slope of the loading curve around a shear angle of 20 degrees, for the Lego/NIPAM hybrid unit cell. From the critical point to the fully deswollen state, the modulus increases by approximately a factor of 4 as a result of prestress.

References

- (1) Damavandi, O. K.; Hagh, V. F.; Santangelo, C. D.; Manning, M. L. Energetic Rigidity. I. A Unifying Theory of Mechanical Stability. *Phys. Rev. E* **2022**, *105* (2), 025003. <https://doi.org/10.1103/PhysRevE.105.025003>.
- (2) Connelly, R.; Whiteley, W. Second-Order Rigidity and Prestress Stability for Tensegrity Frameworks. *SIAM J. Discrete Math.* **1996**, *9* (3), 453–491. <https://doi.org/10.1137/S0895480192229236>.